A Conformational Mimic of the MgATP-Bound "On State" of the Nitrogenase Iron Protein[†,‡]

Sanchayita Sen,[§] Robert Igarashi,[||] Archer Smith,[⊥] Michael K. Johnson,[⊥] Lance C. Seefeldt,[||] and John W. Peters*[,§]

Department of Chemistry and Biochemistry, Montana State University, Bozeman, Montana 59717, Department of Chemistry and Biochemistry, Utah State University, Logan, Utah 84322, and Department of Chemistry and Center for Metalloenzyme Studies, University of Georgia, Athens, Georgia 30602

Received October 13, 2003; Revised Manuscript Received December 16, 2003

ABSTRACT: The crystal structure of a nitrogenase Fe protein single site deletion variant reveals a distinctly new conformation of the Fe protein and indicates that, upon binding of MgATP, the Fe protein undergoes a dramatic conformational change that is largely manifested in the rigid-body reorientation of the homodimeric Fe protein subunits with respect to one another. The observed conformational state allows the rationalization of a model of structurally and chemically complementary interactions that occur upon initial complex formation with the MoFe protein component that are distinct from the protein−protein interactions that have been characterized previously for stabilized nitrogenase complexes. The crystallographic results, in combination with complementary UV−visible absorption, EPR, and resonance Raman spectroscopic data, indicate that the [4Fe-4S] cluster of both the Fe protein deletion variant and the native Fe protein in the presence of MgATP can reversibly cycle between a regular cubane-type [4Fe-4S] cluster in the reduced state and a cleaved form involving two [2Fe-2S] fragments in the oxidized state. Resonance Raman studies indicate that this novel cluster conversion is induced by glycerol, and the crystallographic data suggest that glycerol is bound as a bridging bidentate ligand to both [2Fe-2S] cluster fragments in the oxidized state.

The biochemical apparatus that is responsible for the conversion of atmospheric nitrogen gas to ammonia is the complex metal-containing enzyme nitrogenase. Nitrogenase is a two-component enzyme, and in the most extensively studied of the nitrogenase enzyme systems, a MgATP binding iron−sulfur protein termed the Fe protein serves as the unique electron donor to the MoFe protein where nitrogen is bound and reduced (*1*−*3*). The MoFe protein contains two types of complex metal clusters, the P clusters, which serve as an intermediate acceptor of electrons from the Fe protein on route to the FeMo cofactors, which in turn serve as the sites for substrate binding and reduction.

The Fe protein is a member of a large class of proteins that couple nucleoside triphosphate (either ATP[1] or GTP) binding and hydrolysis to protein conformational changes that can be transduced within a macromolecular complex (*4*, *5*). Members of this class are involved in numerous important cellular processes, including G proteins in hormone-stimulated metabolic activities (*6*, *7*), transducin in the light-driven response in vision (*8*), EF-Tu in protein synthesis (*9*, *10*), RecA in DNA repair (*11*, *12*), and myosin in muscle contraction (*13*−*16*). Individual members of the class can be related and identified by regions of amino acid sequence conservation in the nucleotide binding regions of the proteins. All of the members possess two sets of consensus amino acid sequence motifs termed Walker A and Walker B sequences (*4*, *5*, *17*) (Table 1).

For G protein-coupled receptors, the binding of a hormone at a receptor induces a conformational change in the receptor, resulting in an association with the heterotrimeric G protein. The interaction of the G protein with the receptor imposes conformational changes in the α-subunit of a heterotrimeric G protein (Gα), resulting in nucleotide displacement (MgGTP for MgGDP) and dissociation of Gα in the "on state". The activated Gα can then, for example, act as a positive effector for a specific enzyme involved in metabolism. Modulating between the two macromolecular partners as a function of the nucleotide-bound (MgGDP or MgGTP) state

[†] This work was supported by grants from the U.S. Department of Agriculture (2001-35318-13105 to J.W.P.), the National Science Foundation (MCB-0090187 to L.C.S.), and the National Institutes of Health (GM62542 to M.K.J.). J.W.P. is the recipient of a Camille Dreyfus Teacher/Scholar Award. Portions of this research were carried out at the Stanford Synchrotron Radiation Laboratory, a national user facility operated by Stanford University on behalf of the U.S. Department of Energy, Office of Basic Energy Sciences. The SSRL Structural Molecular Biology Program is supported by the Department of Energy, Office of Biological and Environmental Research, and by the National Institutes of Health, National Center for Research Resources, Biomedical Technology Program, and the National Institute of General Medical Sciences.

[‡] Coordinates have been deposited in the Protein Data Bank (www.rscb.org) under the accession code 1RW4.

* To whom correspondence should be addressed. E-mail: john.peters@chemistry.montana.edu. Voice: 406-994-7211. Fax: 406-994-7212.

[§] Montana State University.

[||] Utah State University.

[⊥] University of Georgia.

[1] Abbreviations: ATP, adenosine 5′-triphosphate; GTP, guanosine 5′-triphosphate; EF-Tu, elongation factor Tu; DNA, deoxyribonucleic acid; GDP, guanosine 5′-diphosphate; ADP, adenosine 5′-diphosphate; PDB, Protein Data Bank; MR, molecular replacement; ARP, automated refinement program; CNS, crystallography and NMR system; EPR, electron paramagnetic resonance; EDTA, ethylenediaminetetraacetic acid; UV, ultraviolet.

10.1021/bi0358465 CCC: $27.50
Published on Web 01/29/2004

Table 1: Sequence Comparison for Walker A and Walker B Motifs of Nucleotide Binding Proteins[a]

protein	process	Walker A	Walker B	nucleotides involved
Fe protein	electron transfer and ATP hydrolysis	**G**K**GG**I**GKS**	DVLG	ATP
Ras protein	cell differentiation	**GAG**GV**GKS**	DTAG	GTP
EF-Tu	protein synthesis	**G**HVDH**GKT**	DGPG	GTP
myosin	muscle contraction	**G**ES**G**A**GKT**	DISGFE	ATP
transducin	vision	GAGES**GKS**	DVGG	GTP
RecA	DNA repair	GPESS**GKT**	VIVVDSV	ATP
eIF4A	protein synthesis	AQSGT**GKT**	DEAD	ATP

[a] Indicated by single letter amino acid code.

requires regions for communication between the nucleotide binding site and the sites for protein−protein interaction, and these regions have been termed nucleotide-dependent switch regions. The "off state" of the G protein is released upon GTP hydrolysis and provides an elegant system of desensitization through a slow inherent GTP hydrolysis activity of the G protein that can be regulated through the association of other proteins that enhance the specific GTPase activity.

The Fe protein is a special member of this class in both form and function, and thus the comparisons of the Fe protein structure and function with other members are very interesting (*1*−*3*). Structurally, the Fe protein, unlike the other members of the class, exists as a dimer with subunits covalently linked by a single [4Fe-4S] cluster. In terms of function, the enzyme utilizes MgATP to define conformational states that allow the Fe protein to make sequential electron transfers to the MoFe protein in a manner that allows electrons to accumulate on the MoFe protein as either electrons residing on the metal clusters or in enzyme-associated substrate reduction intermediates. During nitrogenase catalysis, each Fe protein dimer binds two MgATP molecules and in the reduced state forms a complex in which at least one electron can be transferred to the MoFe protein. The interaction of the on state of the Fe protein with the MoFe protein results in conformational changes imposed on the Fe protein, leading to MgATP hydrolysis and the transition to the MgADP-bound state or the off state. For the Fe protein the aforementioned nucleotide-dependent switch regions link the sites for nucleotide binding and hydrolysis with the Fe protein's [4Fe-4S] cluster and the sites for MoFe protein interaction. This allows for nucleotide-dependent control of nitrogenase complex formation and the redox properties of the Fe protein's [4Fe-4S] cluster. Although the role and absolute requirement for MgATP in nitrogenase catalysis are not completely understood, a potential role is implied in providing a means to accumulate multiple reducing equivalents on either the metal clusters or enzyme-bound reduced intermediates of the substrate on the MoFe protein.

The nitrogenase components have been structurally characterized in their native state as well as a number of defined states relevant to the nitrogenase catalytic cycle (*18*−*25*). The structures of the Fe protein in its native state and MgADP-bound state (*20*, *26*) as well as the nitrogenase Fe protein−MoFe protein complex have contributed significantly to our understanding of the role of MgATP binding and hydrolysis in nitrogenase catalysis. The structure of the nitrogenase complex stabilized in the presence of MgADP and tetrafluoroaluminate (*27*, *28*) revealed that the Fe protein can undergo significant conformational changes during complex formation. Yet to be structurally characterized is the MgATP-bound on state of the Fe protein. The structure of this state is critical to dissecting the protein−protein interactions within the nitrogenase complex that result in the Fe protein conformational changes that trigger MgATP hydrolysis and electron transfer.

Capturing crystals of proteins in the presence of bound nucleoside triphosphates is a difficult task since these compounds are not stable to the extent that they can be incubated at ambient temperatures for extended periods without being hydrolyzed. The instability has been overcome in some systems by utilizing the various nonhydrolyzable analogues of GTP or ATP (*6*, *29*, *30*). A variant of the *Azotobacter vinelandii* Fe protein has been characterized previously in which a single amino acid deletion has been placed in the nucleotide-dependent switch region responsible for communication with the sites for nucleotide binding and hydrolysis and the [4Fe-4S] cluster (*31*, *32*). The Fe protein with a single deletion of Leu at position 127 has been extensively studied and shown to have biochemical and biophysical properties in its nucleotide-free form that mimic the native Fe protein in the presence of bound MgATP (*31*, *32*). In further support of the concept that the L127 deletion variant is a structural mimic of the Fe protein MgATP-bound state, it has been shown that the Fe protein variant forms a tight binding complex with the MoFe protein in either the presence or absence of bound nucleotides (*31*, *33*). This complex has been structurally characterized and significantly resembles the structure of the nitrogenase complex stabilized in the presence of MgADP and tetrafluoroaluminate (*27*, *28*).

MATERIALS AND METHODS

Protein Crystallography. The Leu127 deletion variant of the nitrogenase enzyme was purified from *A. vinelandii* as described previously (*32*). The protein was concentrated to 70 mg/mL prior to crystallization. The conditions for crystallization were initially identified through sparse matrix screens (*34*, *35*). Crystals were grown under anaerobic conditions in a Coy anaerobic chamber using the microcapillary batch diffusion method (*20*) with 24% poly(ethylene glycol), MW = 4000, as the precipitating agent in 0.16 M $MgCl_2$, trishydrochloric acid, pH 8.5, 20% glycerol, and 1 mM sodium dithionite. The crystals are brown in color and grow to the approximate dimensions of 0.2 × 0.5 × 1 mm in ∼2−3 weeks.

Data were collected on beamlines 9-1 and 9-2 of the Stanford Synchrotron Radiation Laboratory, and during data collection the crystals were cooled by a continuous flow of liquid nitrogen at 93 K. The data were processed using MOSFLM (*36*) and scaled using the SCALA (*37*) suite program. For the collection of multiple wavelength anomalous dispersion (MAD) data, absorption edge measurements were utilized to identify the energies of f' and f''. Data sets were collected at the wavelengths corresponding to f' and

Table 2: Multiple Wavelength Anomalous Diffraction Data Statistics

cell dimensions	$a = 70.7$ Å $b = 133.0$ Å $c = 61.1$ Å $\alpha = \beta = \gamma = 90.00°$	space group	$C222_1$

	remote	Fe edge	
	$\lambda_1 = 1.4251$ Å	$\lambda_2 = 1.6934$ Å	$\lambda_3 = 1.7416$ Å
resolution (Å)	50.00−2.96	50.00−2.96	50.00−3.00
completeness (%)	99.5 (99.9)	98.8 (93.6)	99.3 (97.6)
obsd reflections	55579	56685	25479
unique reflections	6172	6042	5745
I/σ	8.2 (5.8)	4.0 (3.0)	4.5 (1.8)
R_{merge}[a]	0.064 (0.109)	0.105 (0.199)	0.107 (0.182)

[a] $R_{merge} = \sum_{hkl}\sum_i|I_i - \langle I\rangle|/\sum_{hkl}\sum_i|\langle I\rangle|$, where I_i is the intensity for the ith measurement of an equivalent reflection with indices h,k,l. Data statistics for the highest resolution shell are indicated in parentheses.

Table 3: Data and Refinement Statistics

data statistics	
resolution (Å)	20.0−2.50
completeness (%)	99.4 (99.8)
observed reflections	122724
unique reflections	10015
I/σ	10.6 (4.7)
R_{merge}[a]	0.059 (0.135)
refinement statistics (8.0−2.5 Å)	
R_{cryst}	0.220
R_{free}	0.272
average B factor (Å^2)	46.2
rms bond (Å)	0.01
rms angles (deg)	2.7

[a] $R_{merge} = \sum_{hkl}\sum_i|I_i - \langle I\rangle|/\sum_{hkl}\sum_i|\langle I\rangle|$, where I_i is the intensity for the ith measurement of an equivalent reflection with indices h,k,l. Data statistics for the highest resolution shell are indicated in parentheses.

f'', and in addition one data set was collected at a wavelength corresponding to an energy remote of the edge. Data statistics for the 3.0 Å MAD data are shown in Table 2.

The structure was determined using a combination of molecular replacement (MR) techniques using AMORE (*38*) and multiple wavelength anomalous dispersion methods (*39*) using the program SOLVE (*40*) for the identification of Fe sites and phase calculation. Preliminary determination of the crystal symmetry and cell parameters indicated the asymmetric unit of the crystals would contain a single subunit of the Fe protein dimer (Table 2) (*41*). For the molecular replacement, a single subunit of the dimeric Leu127 deletion variant of the *A. vinelandii* Fe protein from the complex structure (PDB accession code 1G20) was used as the search model. The initial solution resulted in a correlation coefficient of 0.42 and an R factor of 0.45. Searches for iron sites using the MAD data resulted in the identification of a single iron site with a refined occupancy of ∼2.0 located very close to the crystallographic 2-fold axis. The individual iron sites were tentatively assigned using considerations concerning the limited degrees of freedom that define iron−iron distances in iron−sulfur clusters as previously described (*42*). The refinement of MAD phases using a phase model having two iron atoms yielded a figure of merit of 0.8. Phases from the MAD and MR experiments were combined using ARP/wARP (*43*, *44*), and the model was assigned using iterative cycles of model building using the program O (*45*) and refinement using X-PLOR and CNS (*46*, *47*). For refinement, 5% of the data were set aside for the calculation of the R_{free}, and the data were randomized to validate the R_{free} by simulated annealing using X-PLOR (*15*). During model building, certain regions of the protein were encountered in which the quality of the electron density maps was poor and the model could not unambiguously be assigned. These regions include amino acid residues 60−70, 90−98, and 133−143, most of which happen to be adjacent residues of Cys97 and Cys132 that serve as [Fe-S] cluster ligands. The final model obeys reasonable stereochemistry as evaluated by PROCHECK. Data statistics for the data used in the refinement and the crystallographic refinement statistics are shown in Table 3 and reflect X-PLOR refinement using data from 2.5 to 8.0 Å resolution with a 0σ cut.

Preparation of Samples for Spectroscopic Measurements. All sample manipulations were carried out in a Vacuum Atmospheres glovebox under an Ar atmosphere (<5 ppm O_2). Samples of wild-type and the L127 deletion variant of *A. vinelandii* Fe protein were purified in 50 mM Tris-HCl buffer, pH 8.0, with 1 mM sodium dithionite and 20% (v/v) glycerol. Glycerol and dithionite were removed by gel filtration using a Sephadex G-25 column, and samples were concentrated by Centricon or Amicon ultrafiltration. ATP-bound wild-type samples were prepared by addition of a 4-fold excess of MgATP (Sigma) using a stock solution prepared in the same buffer. Samples were oxidized by addition of aliquots of a concentrated stock solution of thionin until a persistent color change was observed.

Spectroscopic Measurements. UV−visible absorption spectra were recorded under anaerobic conditions in screw-top 1 mm cuvettes using a Shimadzu UV-3101PC spectrophotometer. Resonance Raman spectra were recorded using an Instruments SA Raman or U1000 spectrometer fitted with a cooled RCA 31034 photomultiplier tube with a 90° scattering geometry. Spectra were recorded digitally using photon counting electronics, and improvements in signal-to-noise ratios were achieved by signal-averaging multiple scans. Band positions were calibrated using the excitation frequency and are accurate to ±1 cm^{-1}. Lines from a Coherent Sabre 10-W argon ion laser and plasma lines were removed using a Pellin Broca Prism premonochromator. Using a custom-designed sample cell (*48*), samples under an Ar atmosphere were placed on the end of a coldfinger of an Air Products Displex Model CSA-202E closed cycle refrigerator and cooled to 17 K. X-band (∼9.5 GHz) EPR spectra were recorded on a Bruker ESP-300E EPR spectrometer equipped with an ER-4116 dual-mode cavity and an Oxford Instrument ESR-9 flow cryostat. Resonances were quantified under nonsaturating conditions using a 1 mM CuEDTA standard.

RESULTS AND DISCUSSION

Overall Structure. The L127 deletion variant of the *A. vinelandii* Fe protein provides the means to gain insights into the conformation of the MgATP-bound on state in the absence of bound nucleotides. The structure of the Fe protein Leu127 deletion variant has been determined and refined to 2.5 Å resolution (*49*), providing structural representation approximating the MgATP-bound on state of the nitrogenase Fe protein, and provides the basis for the characterization of the initial interactions of the Fe protein with the MoFe protein that result in macromolecular complex formation,

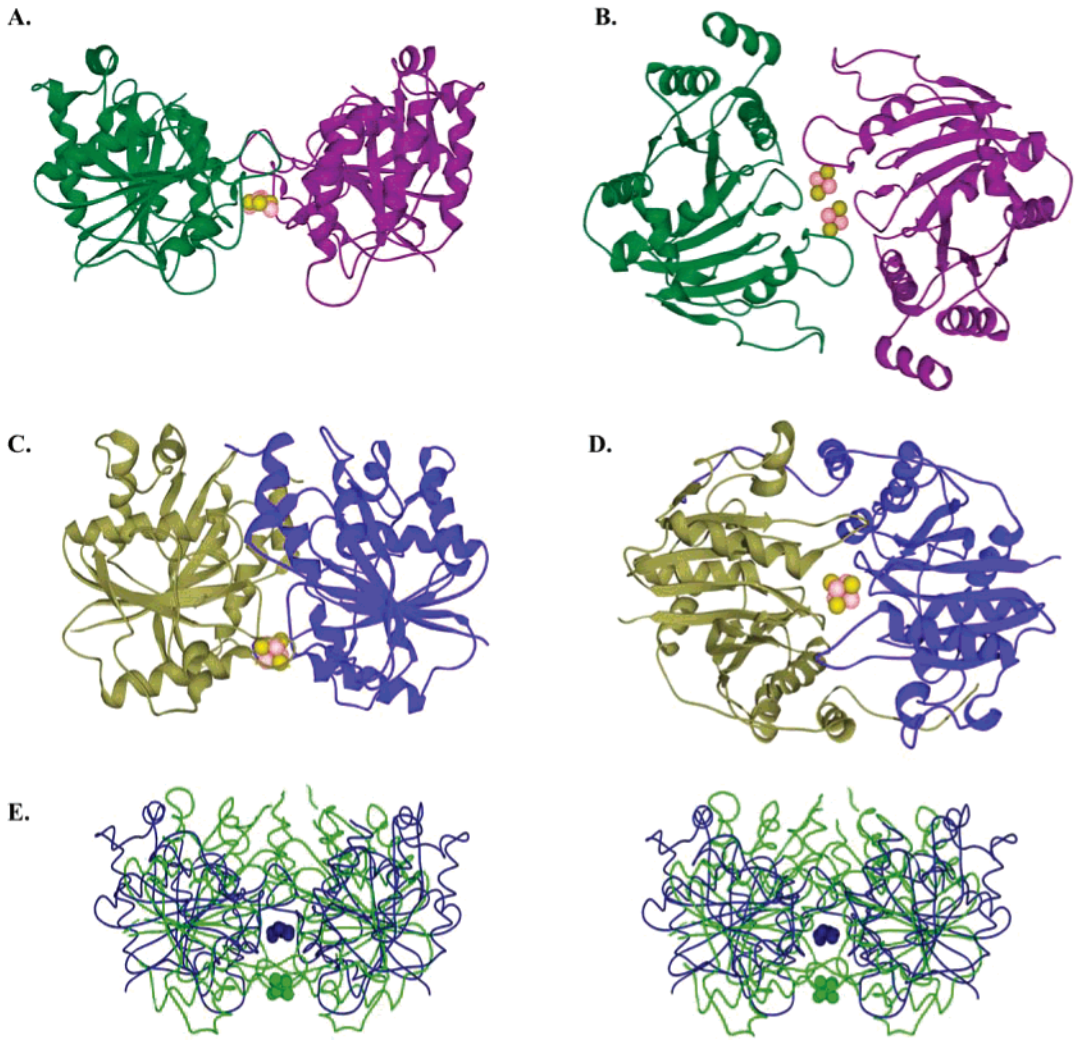

FIGURE 1: Comparison of the overall structural conformations of (A, B) the Fe protein L127 deletion variant with (C, D) the native nitrogenase Fe protein in the absence of bound nucleotides and (E) a wall-eyed stereo figure of the superimposition of the structure of the free L127 deletion variant on the L127 deletion variant from the nitrogenase complex. Views B and D represent a 90° rotation of the views shown in (A) and (C). The [4Fe-4S] clusters are represented in rust (Fe) and yellow (S) spheres.

MgATP hydrolysis, and intermolecular electron transfer. The overall structure of the Fe protein variant reveals a strikingly different protein conformation than observed previously for either the native state (*20*, *50*), the MgADP-bound state (*26*), or the Fe protein conformation observed within the nitrogenase complex structures (*27*, *28*, *33*) (Figure 1). The most significant structural differences that separate the Fe protein variant and the aforementioned structures of the Fe protein are largely manifested in a rigid-body reorientation of the Fe protein subunits with respect to one another. In contrast to the Fe protein within the nitrogenase complexes, it was observed that the Fe protein subunits could undergo a small-scale rigid-body reorientation with respect to one another consisting of approximately 5° for each monomer relative to the Fe protein in its native state. This conformational change resulted in a translation of the Fe protein's [4Fe-4S] cluster toward the Fe protein−MoFe protein docking interface. In the current study, each of the Fe protein subunits is reoriented by a rigid-body rotation with respect to one another on the order of 30° relative to the previously characterized Fe protein structures (*20*, *27*, *33*, *50*). Interestingly, a conformational change on this order has been recently observed in the myosin V motor, which is also a member of the large class of signal transduction proteins. The two heads of the myosin V motor move progressively along an actin filament in a hand over manner, advancing the center of mass by 37 nm for each adenosine triphosphate hydrolyzed (*51*, *52*).

The structures of the individual Fe protein subunits themselves are largely conserved, no doubt a result of the strong interactions provided by the subunits' β-sheet cores. The most pronounced differences occur within the switch II regions near the sites of the deletion mutations and terminate in the covalent attachment provided by the cluster. Presumably the interaction of MgATP with the native Fe protein can result in a similar set of conformational changes through the direct interaction of the Fe protein's phosphate binding loop, "P loop", with the aspartate 129 residues of switch II.

Model for Nitrogenase Component Initial Interactions. The structure provides a basis for understanding the conformation of the Fe protein that interacts productively with the MoFe protein to form a macromolecular complex in which electron transfer and MgATP hydrolysis occur. The Fe protein conformation observed in the L127 deletion variant provides for distinct docking interactions from that observed in the Fe protein−MoFe protein complex structures. The resulting

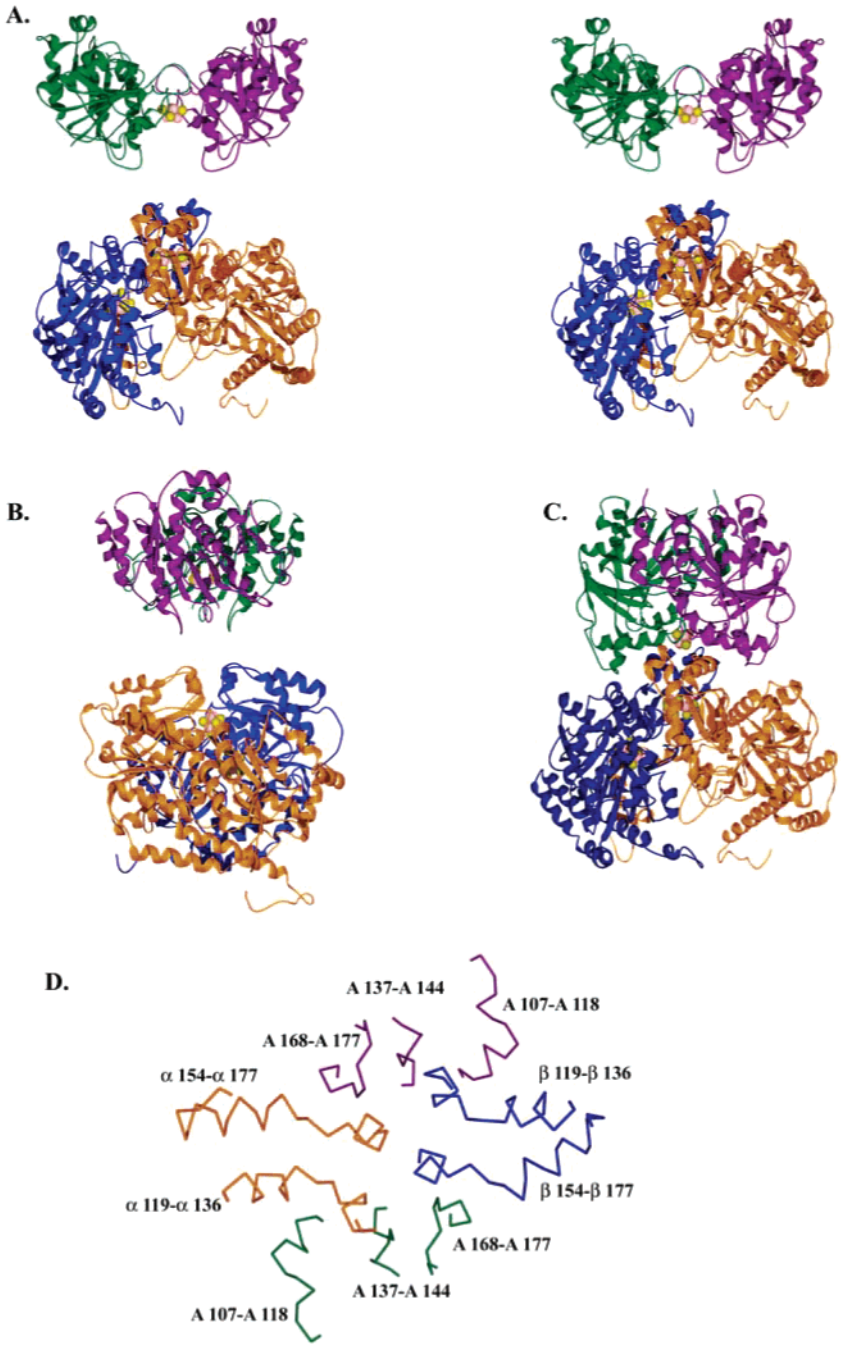

FIGURE 2: Proposed model for initial docking of the L127 Fe protein deletion mutant with the MoFe protein. The docking model is based on structural and chemical complementarities observed at the Fe protein and MoFe protein docking interface. (A) Wall-eyed stereoview of the Fe protein L127 deletion variant poised for initial interaction with an $\alpha\beta$ dimer half of the MoFe protein. (B) A single Fe protein dimer is poised for docking with an $\alpha\beta$ dimer half of the MoFe protein as in (A) rotated 90°. (C) Docking and protein−protein interactions observed in the stable nitrogenase complex formed between the Fe protein L127 deletion variant and the MoFe protein. (D) Cutaway view of the specific Fe protein and MoFe protein regions proposed to interact during initial docking. The structural fit within the docking region of the α-helical region of the MoFe protein docking interface and the loop regions of the Fe protein are represented in the same color scheme as in panels A−C.

conformation can be easily docked as a rigid body with the MoFe protein with both structural and chemical complementary interactions. A docking model can be proposed through the rigid-body docking of the structure on the basis of the pairing of the Fe protein 2-fold axis of symmetry with the pseudo-2-fold symmetric axis of an $\alpha\beta$ dimer of the MoFe protein heterotetramer as observed in the nitrogenase complex structures (Figure 2). The resulting docking model presented here indicates that the nitrogenase docking interactions initially occur by the embrace of loop regions of the Fe protein with the pair of α-helices (present in both the α- and β-subunits) that make up a ridge on the surface of the docking interface of the MoFe protein. The chemical aspect of this docking interaction can be explained on the basis of a large number of potential electrostatic, polar, and hydrophobic interactions that can be realized when the proteins are allowed to dock in the manner described above. As summarized in Table 4, these interactions are quite different from the interactions observed in the nitrogenase complex structures. An example of the potential interactions that can

Table 4: Fe Protein−MoFe Protein Interactions Observed in Nitrogenase Complexes and Implied through Analysis of the Docking Model for Initial Interaction of the Fe Protein L127 Deletion Variant and the MoFe Protein[a]

Fe protein L127Δ−MoFe protein complex	Fe protein L127Δ (ATP)−MoFe protein complex	Fe protein (ADP·AlF_4^-)−MoFe protein complex	free Fe protein L127Δ−MoFe protein docking model
A62−Kα121			D68−αK129
C97−Vα124	C97−Vα124	C97−Vα124	I103−αF125
R100−Eα120	R100−Eα120	R100−Eα120	D141−αR187
R100−Gα157	R100−Gα157	R100−Gα157	Q145−αR203
T104−Eα120	T104−Eα120	R100−Eα184	K170−αD162
R140−Gα160		G133−Iα159	K170−αD161
E141−Kα168			A172−Iα158
			A172−Iα159
C97−Vβ124	C97−Vβ124	C97−Vβ124	D68−βK132
R100−Eβ120	R100−Eβ120	R100−Eβ156	I103−βF125
T104−Eβ120	T104−Eβ120	T104−Eβ120	D141−βH185
R100−Eβ156	R100−Eβ156	G133−Iβ158	Q145−βR206
G133−Iβ158	E111−Kβ303	K170−Nβ168	K170−βD160
R140−Gβ159			A172−Iβ158

[a] All amino acids are indicated by single letter code. Some interactions are supplied by the side chain moieties and some by main chain groups.

be rationalized through analysis of the docking model includes the interaction of glutamate residues within the switch I region of the Fe protein (glutamate 68) directly with a pair of pseudosymmetrically related lysine residues on the α- and β-subunits of the MoFe protein (α-Lys129 and β-Lys132). These interactions could presumably provide the sites that communicate the trigger signal complex formation to the sites for MgATP hydrolysis. Interestingly, mutagenesis studies involving the substitution of a set of nearby surface-exposed Phe residues (α-Phe125 and β-Phe125) by alanine result in a MoFe protein that is unable to promote Fe protein MgATP hydrolysis or participate in nitrogenase complex formation (*53*).

Implied by the comparison of the structure of the free Fe protein L127 deletion variant presented here and the Fe protein structure observed in the complex is that the rather dramatic structural differences observed result from conformational changes imposed on the Fe protein by the MoFe protein interactions that occur during macromolecular complex formation. It was observed in the nitrogenase complex structures that although conformational changes are clearly evident within the Fe protein, MoFe protein conformational differences are restricted to the reorientation of amino acid side chains that are involved with specific protein−protein interactions.

The current study does not preclude the potential for a MoFe protein conformational change occurring during catalysis. However, the conformational changes implied could provide a mechanism for the MoFe protein as a rigid body, providing the interactions critical for intermolecular electron transfer and MgATP hydrolysis. The conformational differences suggest that electron transfer could be facilitated by the repositioning of the Fe protein's [4Fe-4S] cluster, providing for a closer proximity to the MoFe protein's P cluster. In addition, as suggested from the nitrogenase complex structures, the reorientation of the Fe protein's subunits with respect to one another provides the potential for cross-subunit interactions that could participate in the stabilization of intermediates of MgATP hydrolysis, thereby accelerating the hydrolysis event. In sum, this line of thinking provides the basis for MoFe protein catalyzed coordination of electron transfer and MgATP hydrolysis events and the subsequent transition of the Fe protein to the oxidized MgADP-bound off state.

Structure and Environment of the [Fe−S] Cluster. The dramatic conformational differences have significant implications for conformational changes in the environment of the Fe protein's Fe-S cluster during catalysis and provide the basis for an elegant mechanism of modulating the biophysical properties of the cluster. The Fe-S cluster of the Fe protein L127 deletion variant is a great deal more solvent exposed than in the previous structurally characterized states of the Fe protein (*20*, *27*, *33*, *50*). Since we believe the conformational state to strongly resemble that of the native MgATP-bound state of the Fe protein, the large degree of cluster solvent accessibility observed here explains in part the increased sensitivity to metal chelation observed for the native Fe protein in the presence of MgATP (*54*). Although conformational changes in the environment of the Fe protein's [4Fe-4S] cluster were anticipated, changes in the structure of the cluster itself were unexpected. Even at a very early stage of the structure determination it was clearly evident that the Fe-S cluster was structurally distinct from the regular [4Fe-4S] cubane observed in all previous structures of the Fe protein (Figure 3A). The [4Fe-4S] cluster is clearly divided or split into two [2Fe-2S] rhombs (Figure 3B−D). Although the cluster region in the structure of the L127 deletion variant is significantly disordered, the best fit for the coordination environment indicates that each [2Fe-2S] fragment is coordinated by two Cys ligands and nonprotein ligands that include an Fe bridging water molecule and a glycerol molecule that is coordinated in a bidentate-bridging fashion to the Fe atoms of each [2Fe-2S] fragment. The Cys coordination is arranged with each [2Fe-2S] rhomb coordinated by Cys residues from each subunit such that the independent [2Fe-2S] clusters covalently link the subunits of the Fe protein dimer. The rationale for including glycerol as a cluster ligand was initially provided by resonance Raman studies, which indicate that the cluster transformation is specifically induced by glycerol; see below. In addition, the resonance Raman studies presented below indicate that the observed disorder is likely a result of the cluster existing in a mixture of the two [2Fe-2S] and [4Fe-4S] forms within the crystal.

Spectroscopic Characterization of the Fe-S Cluster in the L127 Deletion Variant and ATP-Bound Wild-Type Fe Protein. The unexpected crystallographic results for the structure of the Fe-S cluster in the L127 deletion variant prompted detailed spectroscopic characterization to assess if the crystallographically defined cluster transformation occurs in solution and to evaluate the factors responsible for effecting any cluster transformations observed in solution. In the absence of glycerol, UV−visible absorption, EPR, and resonance Raman studies of the L127 deletion variant provided no clear indication of the novel type of cluster transformation observed by crystallography in either the dithionite-reduced or thionin-oxidized redox states. EPR studies of dithionite-reduced samples revealed a near-axial $S = {}^1/_2$ resonance, $g = 2.03, 1.92, 1.87$, accounting for 0.6 spin/dimeric Fe protein and a weak feature at $g \sim 5$,

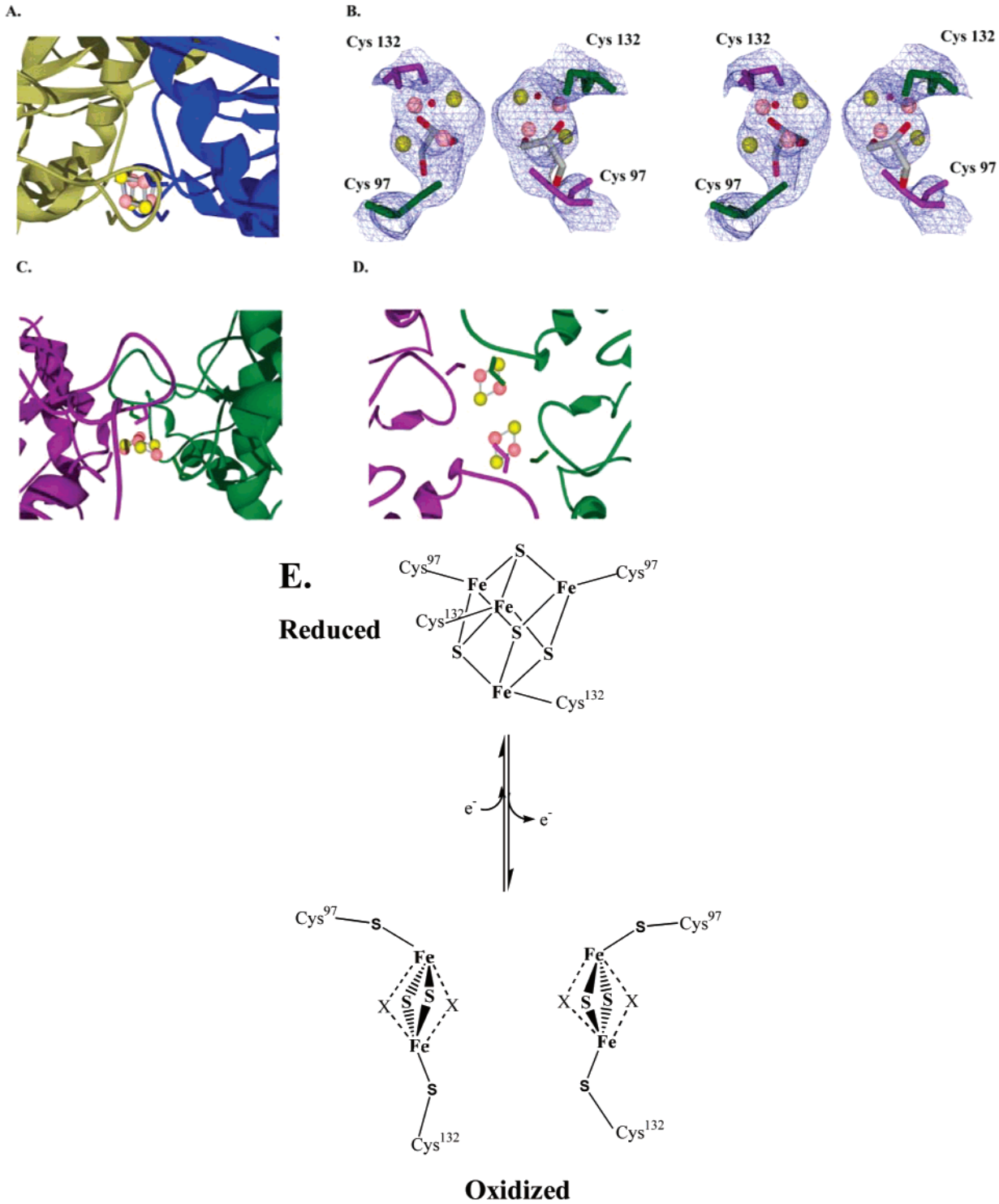

FIGURE 3: (A) Close-up of the environment of the [4Fe-4S] cluster of the native nitrogenase Fe protein in the analogous orientation as view in Figure 1C. (B) Wall-eyed stereoview of $2F_o - F_c$ electron density maps of the [FeS] cluster environment of the Fe protein L127 deletion variant observed in the structure. Nonprotein ligands which could exist as hydroxo or aquo, and as it has been modeled in (B), glycerol molecules are shown. (C, D) Close-up of the structural environment of the [FeS] clusters of the Fe protein L127 deletion variant. The orientations (C and D) shown are analogous to the views of the Fe protein variant shown in Figure 1A,B. (E) Model for the redox-dependent structural changes observed in the Fe protein L127 deletion variant and the native Fe protein with bound MgATP. Nonprotein ligands modeled glycerol and water molecules in (B) are indicated by X.

indicative of a minor $S = {}^3/_2$ component. In accord with previous results (*32*, *55*), these EPR properties are consistent with a mixed-spin $[4Fe\text{-}4S]^+$ cluster in the ATP-bound form of the Fe protein. Oxidation with a minimal excess of thionin after removal of excess dithionite resulted in loss of the EPR signals and conversion of the featureless, monotonically increasing UV−visible absorption into a spectrum with a well-defined shoulder at ~400 nm. Both changes are consistent with oxidation to a $S = 0$ $[4Fe\text{-}4S]^{2+}$ cluster.

Resonance Raman, which provides a more discriminating method for distinguishing between clusters with $S = 0$ ground states, revealed the presence of both $[4Fe\text{-}4S]^{2+}$ and

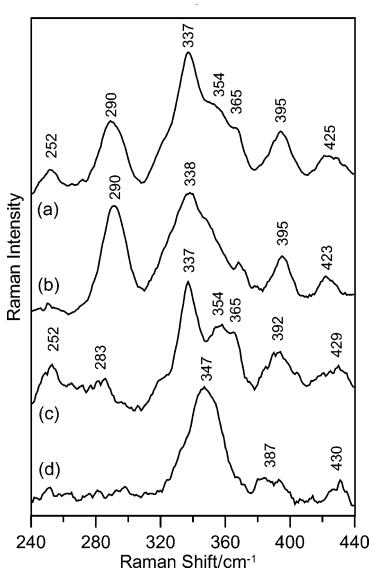

FIGURE 4: Resonance Raman spectra of thionin-oxidized samples of the L127 deletion variant of *A. vinelandii* Fe protein: (a) oxidized after removal of glycerol; (b) sample in (a) treated with a 5-fold stoichiometric excess of EDTA; (c) difference spectrum, (a) minus (b); (d) oxidized in the presence of 30% (v/v) glycerol. Samples were all ~3 mM in Fe protein and were oxidized anaerobically after removal of dithionite using a 2-fold stoichiometric excess of thionin. Spectra were recorded at 17 K, using 457.9 nm excitation, by photon counting for 1 s every 1 cm^{-1}. Each spectrum is the sum of 90−100 scans. Bands originating from lattice modes of ice, glycerol, and oxidized thionin have been subtracted.

$[2Fe\text{-}2S]^{2+}$ clusters in thionin-oxidized samples of the L127 deletion variant (Figure 4a). Similar spectra have been observed and analyzed in detail for thionin-oxidized wild-type Fe protein in the presence of MgATP (see below and ref *56*). Moreover, as for the oxidized ATP-bound Fe protein, the spectrum of the $[2Fe\text{-}2S]^{2+}$ center in isolation was obtained by treating the sample with a metal ion chelator such as EDTA (Figure 4b). The ability to selectively remove two Fe atoms from oxidized ATP-bound Fe protein by the addition of metal chelators to form a semistable derivative with one $[2Fe\text{-}2S]^{2+}$ cluster bound per dimer is well documented (*54*). Hence the oxidized L127 deletion variant is shown to mimic oxidized ATP-bound wild-type Fe protein, in terms of the mechanism of oxidative cluster degradation via a semistable $[2Fe\text{-}2S]^{2+}$ intermediate. Subtraction of the contribution from the $[2Fe\text{-}2S]^{2+}$ cluster, after normalization of the intensities of the isolated $[2Fe\text{-}2S]^{2+}$ cluster bands at 290 cm^{-1}, results in a resonance Raman spectrum characteristic of a $[4Fe\text{-}4S]^{2+}$ cluster (Figure 4c) that is attributed to the ATP-bound form of the oxidized Fe protein with the $[4Fe\text{-}4S]^{2+}$ intact. Since the intensities of the resonance Raman spectra of $[2Fe\text{-}2S]^{2+}$ centers are typically 5−10 times greater than those of $[4Fe\text{-}4S]^{2+}$ centers with 457.9 nm excitation (*56*−*58*), the $[2Fe\text{-}2S]^{2+}$ cluster-containing form is likely to be a minor component and hence not readily evident in the UV−visible absorption spectrum. While it is not possible to rule out the possibility that the minor $[2Fe\text{-}2S]^{2+}$ cluster-containing component is related to the novel [2Fe-2S] fragments observed by crystallography, the spectroscopic studies clearly indicate that the form with an intact $[4Fe\text{-}4S]^{2+}$ cluster is the dominant component in the Fe protein L127 deletion variant oxidized in the absence of glycerol.

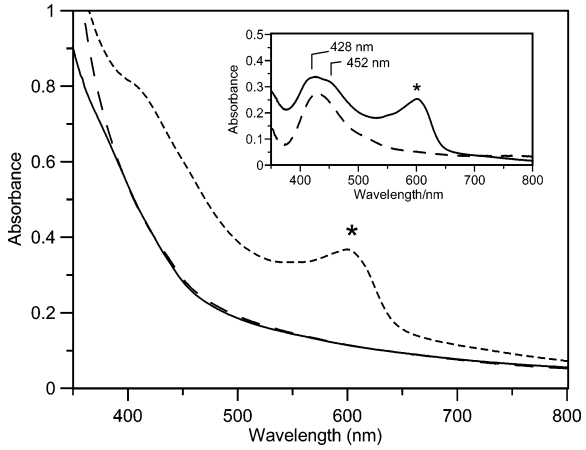

FIGURE 5: Absorption spectra of thionin-oxidized and dithionite-reduced samples of the L127 deletion variant of *A. vinelandii* Fe protein in the presence of 20% (v/v) glycerol. The as prepared reduced sample after anaerobic removal of dithionite (solid line) was oxidized with excess thionin (dashed line) and rereduced with excess dithionite (broken line). The inset shows thionin-oxidized minus the as prepared reduced difference spectra in the absence (broken line) and presence (solid line) of 20% glycerol. Bands originating from excess thionin are indicated by an asterisk.

Very different spectroscopic results in the oxidized state were observed for samples of the Fe protein L127 deletion variant that were oxidized in the presence of 20−30% (v/v) glycerol, conditions similar to those used for crystallization. Samples oxidized in the presence of glycerol remained EPR silent. However, the resonance Raman of thionin-oxidized samples in the presence of 30% (v/v) glycerol is completely different, with a broad intense band at 347 cm^{-1} and weak bands at 387 and 430 cm^{-1} (Figure 4d). A similar spectrum was observed with 20% (v/v) glycerol, except for the presence of a shoulder at 337 cm^{-1} and weak bands at 252 and ~280 cm^{-1}, indicating the presence of some $[4Fe\text{-}4S]^{2+}$ clusters. The absorption spectrum is also somewhat different, with the broad shoulder red shifted to ~420 nm, in samples treated with 20% (v/v) glycerol (Figure 5). The glycerol-induced change in the absorption spectrum is more clearly evident in the oxidized minus reduced difference spectrum shown in the inset to Figure 5. In contrast, the reduced state is not significantly perturbed by the presence of glycerol. Addition of 20% (v/v) glycerol does not perturb the reduced absorption spectrum, and the EPR spectrum is essentially unchanged except that quantitative studies indicate a small change in the spin state mixture in favor of the $S = {}^1/_2$ component, which increases from 0.6 to 0.8 spin/dimeric Fe protein. Of particular importance is the observation that the redox-induced change is reversible, as evidenced by near quantitative recovery of the reduced absorption and EPR properties following an oxidation/reduction cycle (Figure 5).

The dramatic changes in the resonance Raman properties of the oxidized L127 deletion variant in the presence of glycerol prompted parallel studies of the ATP-bound form of the wild-type Fe protein (Figure 6). In the absence of glycerol, the spectra of the thionin-oxidized wild-type Fe protein in the absence and presence of MgATP (spectra a and b of Figure 6, respectively) are in excellent agreement with previously published results (*56*). ATP binding results in some degradation of the $[4Fe\text{-}4S]^{2+}$ cluster to the semistable $[2Fe\text{-}2S]^{2+}$ cluster-containing form as evidenced by the appearance of the 290 cm^{-1} band. The resonance

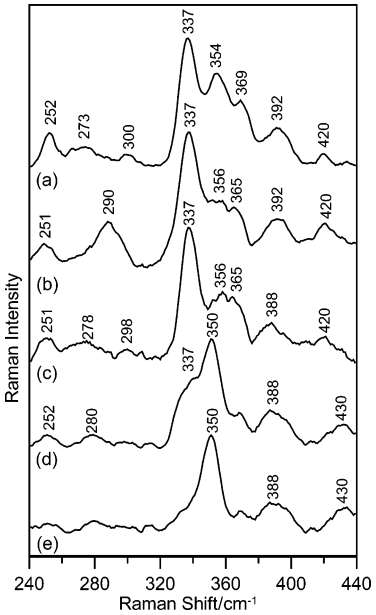

FIGURE 6: Resonance Raman spectra of thionin-oxidized samples of wild-type *A. vinelandii* Fe protein: (a) oxidized after removal of glycerol; (b) sample in (a) treated with a 4-fold stoichiometric excess of MgATP; (c) difference spectrum, (b) minus contribution from $[2Fe\text{-}2S]^{2+}$-containing wild-type Fe protein (analogous to the spectrum shown in Figure 4b); (d) sample in (a) treated with 30% (v/v) glycerol and a 4-fold stoichiometric excess of MgATP; (e) difference spectrum, (d) minus (c). Samples were all ~3 mM in Fe protein and were oxidized anaerobically after removal of dithionite using a 2-fold stoichiometric excess of thionin. Spectra were recorded at 17 K, using 457.9 nm excitation, by photon counting for 1 s every 1 cm^{-1}. Each spectrum is the sum of 90−100 scans. Bands originating from lattice modes of ice, glycerol, and oxidized thionin have been subtracted.

Raman spectrum of the $[4Fe\text{-}4S]^{2+}$ center that is present in the vast majority of the ATP-bound sample (Figure 6c) was therefore obtained by subtraction of the $[2Fe\text{-}2S]^{2+}$ component using the spectrum obtained after addition of EDTA (spectrum not shown but very similar to that in Figure 4b). Comparison of spectra a and c shown in Figure 6 indicates that ATP binding occurs without any major structural perturbation of the $[4Fe\text{-}4S]^{2+}$ in the oxidized Fe protein. However, as for the L127 deletion variant, major changes were apparent in samples treated with 30% (v/v) glycerol (Figure 6d). The conversion is not as extensive as in the L127 deletion variant, as evidenced by significant contributions from bands at 252, 280, and 337 cm^{-1} from the cuboidal $[4Fe\text{-}4S]^{2+}$ cluster. Nevertheless, subtraction of the spectrum corresponding to the $[4Fe\text{-}4S]^{2+}$ center in the oxidized ATP-bound sample (Figure 6c) results in a spectrum with bands at 350, 388, and 430 cm^{-1} (Figure 6e) that is very similar to that observed for the oxidized L127 deletion variant in the presence of 30% (v/v) glycerol (Figure 4d). Hence the novel cluster transformation that is induced by glycerol in the oxidized L127 deletion variant is also observed in oxidized wild-type samples in the presence of ATP.

The spectroscopic evidence for medium-dependent variability in the structure and properties of the Fe protein Fe-S center only in oxidized forms of the ATP-bound wild type and L127 deletion variant indicates that the crystallographic data correspond to an oxidized form of the L127 deletion variant. Moreover, taken together, the spectroscopic and crystallographic results indicate that cleavage of the $[4Fe\text{-}4S]^{2+}$ cluster into two [2Fe-2S] fragments is specifically induced by glycerol and that this cluster transformation is reversed on reduction back to the $[4Fe\text{-}4S]^{+}$ redox state. Since the semistable $[2Fe\text{-}2S]^{2+}$ cluster species is not observed in any of the samples oxidized in the presence of glycerol, our current working hypothesis is that the novel split form of the $[4Fe\text{-}4S]^{2+}$ cluster corresponds to a glycerol-stabilized intermediate in the oxidative degradation pathway that precedes the semistable $[2Fe\text{-}2S]^{2+}$ intermediate. The resonance Raman characteristics of the novel split form of the $[4Fe\text{-}4S]^{2+}$ cluster are unique in our experience, which makes it difficult to reach a definitive conclusion concerning the redox state of the [2Fe-2S] fragments. We have considered three possibilities: a diferric pair, a valence-localized mixed-valence pair, and a valence-delocalized mixed-valence pair. While the extensive absorption and resonance Raman data for the first two possibilities in simple $[2Fe\text{-}2S]^{2+,+}$ ferredoxins bear little resemblance to that reported here for the novel split form of the $[4Fe\text{-}4S]^{2+}$ cluster (*57*, *59*, *60*), it must be borne in mind that none of these ferredoxins have a single cysteine ligating both Fe atoms. In contrast, although the absorption and resonance Raman data for valence-delocalized $S = {}^9/_2$ $[2Fe\text{-}2S]^{+}$ clusters are restricted to the C56S and C60S variants of *Clostridium pasteurianum* 2Fe ferredoxin (*61*), the spectra do show some similarity to those of the [2Fe-2S] fragments in the Fe protein. These valence-delocalized $[2Fe\text{-}2S]^{+}$ clusters exhibit absorption spectra with shoulders at 420 and 470 nm and a weaker lower energy band at 670 nm and resonance Raman spectra that are dominated by the symmetric breathing mode of the $Fe_2(\mu_2\text{-}S)_2$ unit at 368 cm^{-1} and a weaker asymmetric stretching mode of the $Fe_2(\mu_2\text{-}S)_2$ unit at 385 cm^{-1}. Hence we tentatively conclude that the two fragments are cleaved without oxidation or disruption of the valence delocalization within each $[2Fe\text{-}2S]^{+}$ unit and that the lack of an EPR signal is a consequence of antiferromagnetic coupling between the two $S = {}^9/_2$ $[2Fe\text{-}2S]^{+}$ units which are separated by approximately 5 Å. Mössbauer experiments are planned to test this hypothesis.

CONCLUSIONS

The results described herein contribute significantly to our understanding of the role of the nucleoside triphosphate-dependent signal transduction mechanism in nitrogenase catalysis. The spectroscopic studies presented, as well as complementary docking interactions that can be rationalized, provide overwhelming support for the proposal that the L127 deletion variant of the Fe protein provides a faithful biochemical and structural mimic of the native MgATP-bound state of the Fe protein (*31*−*33*). In terms of nitrogenase catalysis, the structure provides the first basis for rationalization of the initial docking interactions contributing to understanding not only the protein conformational changes that occur upon nucleotide binding but also those conformational changes imposed onto the Fe protein by the MoFe protein during complex formation. These conformational changes specifically result in electron transfer and MgATP hydrolysis in the nitrogenase complex.

The glycerol-induced cleavage of the $[4Fe\text{-}4S]^{2+}$ cluster to yield two [2Fe-2S] fragments appears to be a direct consequence of increased solvent exposure in the ATP-bound conformation of the Fe protein. However, the spectroscopic

evidence for regular cuboidal $[4Fe\text{-}4S]^{2+}$ centers as the dominant form of the cluster in the ATP-bound conformations of both the wild-type and variant oxidized Fe proteins in the absence of glycerol argues strongly against any physiological relevance for this cluster transformation. Rather it appears to correspond to a trapped intermediate that precedes the formation of the semistable $[2Fe\text{-}2S]^{2+}$ intermediate in the biphasic oxidative decomposition of the $[4Fe\text{-}4S]^{2+}$ cluster (*54*). Nevertheless, this type of cluster transformation has not been observed previously in a biological system and is likely to be relevant to understanding the mechanism of oxidative cluster degradation of $[4Fe\text{-}4S]^{2+}$ clusters in the radical−SAM family of Fe-S enzymes and to the mechanism of biosynthesis of $[4Fe\text{-}4S]^{2+}$ clusters. The $[4Fe\text{-}4S]^{2+,+}$ clusters that mediate reductive cleavage of *S*-adenosyl-L-methionine to yield 5′-deoxyadenosyl radicals are known to undergo oxidative degradation via a $[2Fe\text{-}2S]^{2+}$ cluster with resonance Raman properties almost identical to those of the semistable $[2Fe\text{-}2S]^{2+}$ intermediate observed during oxidative degradation of the Fe protein in the ATP-bound conformation (*62*−*64*). Reductive coupling of adjacent [2Fe-2S] clusters has been invoked to explain the biosynthesis of [4Fe-4S] clusters on apo Fe-S proteins and on proteins such as IscU, IscA, and NifU that function as scaffolds for Fe-S cluster biosynthesis (*65*−*67*). The current study provides the first structurally characterized example of this coupling mechanism occurring in a biological system.

REFERENCES

1. Howard, J. B., and Rees, D. C. (1994) Nitrogenase: A nucleotide-dependent molecular switch, *Annu. Rev. Biochem. 63*, 235−264.
2. Rees, D. C., and Howard, J. B. (2000) Nitrogenase: standing at the crossroads, *Curr. Opin. Chem. Biol. 4*, 559−566.
3. Seefeldt, L. C., and Dean, D. R. (1997) Role of nucleotides in nitrogenase catalysis, *Acc. Chem. Res. 30*, 260−266.
4. Koonin, E. V. (1993) A superfamily of ATPases with diverse functions containing either classical or deviant ATP-binding motifs, *J. Mol. Biol. 229*, 1165−1174.
5. Schulz, G. E. (1992) Binding of nucleotides by proteins, *Curr. Opin. Struct. Biol. 2*, 61−67.
6. Sprang, S. R. (1997) G protein mechanisms: Insights from structural analysis, *Annu. Rev. Biochem. 66*, 639−678.
7. Sunahara, R. K., Tesmer, J. J., Gilman, A. G., and Sprang, S. R. (1997) Crystal structure of the adenylate cyclase activiator Gsγ, *Science 278*, 1943−1947.
8. Sondek, J., Lambright, D. G., Noel, J. P., Hamm, H. E., and Sigler, P. B. (1994) GTPase mechanisms of G proteins from the 1.7 Å structure of transducin alpha-GDP-AlF_4^-, *Nature 372*, 276−279.
9. Kjeldgaard, M., and Nyborg, J. (1992) Refined structure of elongation factor EF-Tu from *Escherichia coli*, *J. Mol. Biol. 223*, 721−742.
10. Jurnak, F. (1985) Structure of the GDP domain of EF-Tu and location of the amino acids homologous to ras oncogene proteins, *Science 230*, 32−36.
11. Story, R. M., and Steitz, T. A. (1992) Structure of the recA protein-ADP complex, *Nature 355*, 374−376.
12. Story, R. M., Weber, I. T., and Steitz, T. A. (1992) The structure of the *E. coli* recA protein monomer and polymer, *Nature 355*, 318−325.
13. Rayment, I. (1996) The structural basis of the myosin ATPase activity, *J. Biol. Chem. 271*, 15850−15853.
14. Rayment, I., and Holden, H. M. (1994) The three-dimensional structure of a molecular motor, *Trends Biochem. Sci. 19*, 129−134.
15. Rayment, I., Holden, H. M., Whittaker, M., Yohn, C. B., Lorenz, M., Holmes, K. C., and Milligan, R. A. (1993) Structure of the actin-myosin complex and its implication for muscle contraction, *Science 261*, 58−65.
16. Rayment, I., Rypniewski, W. R., Schmidt-Base, K., Smith, R., Tomchick, D. R., Benning, M. M., Winkelmann, D. A., Wesenberg, G., and Holden, H. M. (1993) Three-dimensional structure of myosin subfragment-1: a molecular motor, *Science 261*, 50−58.
17. Robson, R. L. (1984) Identification of possible adenine nucleotide-binding sites in nitrogenase Fe- and MoFe-proteins by amino acid sequence comparison, *FEBS Lett. 173*, 394−398.
18. Bolin, J. T., Ronco, A. E., Morgan, T. V., Mortenson, L. E., and Xuong, N. (1993) The unusual metal clusters of nitrogenase: structural features revealed by X-ray anomalous diffraction studies of the MoFe protein from *Clostridium pasteurianum*, *Proc. Natl. Acad. Sci. U.S.A. 90*, 1078−1082.
19. Chan, M. K., Kim, J., and Rees, D. C. (1993) The nitrogenase FeMo-cofactor and P-cluster pair: 2.2 Å resolution structures, *Science 260*, 792−794.
20. Georgiadis, M. M., Komiya, H., Chakrabarti, P., Woo, D., Kornuc, J. J., and Rees, D. C. (1992) Crystallographic structure of the nitrogenase iron protein from *Azotobacter vinelandii*, *Science 257*, 1653−1659.
21. Kim, J., and Rees, D. C. (1992) Crystallographic structure and functional implications of the nitrogenase molybdenum iron protein from *Azotobacter vinelandi*, *Nature 360*, 553−560.
22. Kim, J., and Rees, D. C. (1992) Structural models for the metal centers in the nitrogenase molybdenum−iron protein, *Science 257*, 1677−1682.
23. Kim, J., Woo, D., and Rees, D. C. (1993) X-ray crystal structure of the nitrogenase molybdenum−iron protein from *Clostridium pasteurianum* at 3.0-Å resolution, *Biochemistry 32*, 7104−7015.
24. Mayer, S. M., Lawson, D. M., Gormal, C. A., Roe, S. M., and Smith, B. E. (1999) New insights into structure−function relationships in nitrogenase: A 1.6 angstrom resolution X-ray crystallographic study of *Klebsiella pneumoniae* MoFe-protein, *J. Mol. Biol. 292*, 871−891.
25. Peters, J. W., Stowell, M. H., Soltis, S. M., Finnegan, M. G., Johnson, M. K., and Rees, D. C. (1997) Redox-dependent structural changes in the nitrogenase P-cluster, *Biochemistry 36*, 1181−1187.
26. Jang, S. B., Seefeldt, L. C., and Peters, J. W. (2000) Insights into nucleotide signal transduction in nitrogenase: structure of an iron protein with MgADP bound, *Biochemistry 39*, 14745−14752.
27. Schindelin, H., Kisker, C., Schlessman, J. L., Howard, J. B., and Rees, D. C. (1997) Structure of ADP·AlF_4^--stabilized nitrogenase complex and its implications for signal transduction, *Nature 387*, 370−376.
28. Schmid, B., Einsle, O., Chiu, H. J., Willing, A., Yoshida, M., Howard, J. B., and Rees, D. C. (2002) Biochemical and structural characterization of the cross-linked complex of nitrogenase: comparison to the ADP−AlF_4-stabilized structure, *Biochemistry 41*, 15557−15565.
29. Fisher, A. J., Smith, C. A., Thoden, J. B., Smith, R., Sutoh, K., Holden, H. M., and Rayment, I. (1995) X-ray structures of the myosin motor domain of *Dictyostelium discoideum* complexed with MgADP−BeF_x and MgADP−AlF_4, *Biochemistry 34*, 8960−8972.
30. Gulick, A. M., Bauer, C. B., Thoden, J. B., Pate, E., Yount, R. G., and Rayment, I. (2000) X-ray structures of the Dictyostelium discoideum myosin motor domain with six non-nucleotide analogs, *J. Biol. Chem. 275*, 398−408.
31. Lanzilotta, W. N., Fisher, K., and Seefeldt, L. C. (1996) Evidence for electron transfer from the nitrogenase iron protein to the molybdenum−iron protein without MgATP hydrolysis: Characterization of a tight protein−protein complex, *Biochemistry 35*, 7188−7196.
32. Ryle, M. J., and Seefeldt, L. C. (1996) Elucidation of MgATP signal transduction pathway in the nitrogenase iron protein: formation of a conformation resembling the MgATP-bound state by protein engineering, *Biochemistry 35*, 4766−4775.
33. Chiu, H., Peters, J. W., Lanzilotta, W. N., Ryle, M. J., Seefeldt, L. C., Howard, J. B., and Rees, D. C. (2001) MgATP-bound and nucleotide-free structures of a nitrogenase protein complex between the Leu 127 Δ-Fe-protein and the MoFe-protein, *Biochemistry 40*, 641−650.
34. Cudney, B., Patel, S., Weisgraber, K., and Newhouse, Y. (1994) Screening and optimization strategies for macromolecular crystal growth, *Acta Crystallogr., Sect. D: Biol. Crystallogr. 50*, 4114−4123.
35. Jancarik, J., and Kim, S. H. (1991) Sparse matrix sampling: a screening method for crystallization of proteins, *J. Appl. Crystallogr. 24*, 409−411.

36. Leslie, A. G. W. (1992) Recent changes to the MOSFLM package for processing film and imaging plate data, in *Joint CCP4 and ESF-EACBM newsletter on protein crystallography*.
37. Collaborative Computational Project (1994) The CCP4 suite: programs for protein crystallography, *Acta Crystallogr. D50*, 760−763.
38. Navaza, J. (1994) AMORE-an automated package for molecular replacement, *Acta Crystallogr. A50*, 157−163.
39. Hendrickson, W. A. (1991) Determination of macromolecular structures from anomalous diffraction of synchrotron radiation, *Science 254*, 51−58.
40. Terwilliger, T. C., and Berendzen, J. (1999) Automated structure solution of MIR and MAD, *Acta Crystallogr., Sect. D: Biol. Crystallogr. 55*, 849−861.
41. Matthews, B. W. (1968) Solvent content of protein crystals, *J. Mol. Biol. 33*, 491−497.
42. Peters, J. W., and Bellamy, H. D. (1999) Extension of Fe MAD phases in the structure determination of a multiple [FeS] cluster containing hydrogenase, *J. Appl. Crystallogr. 32*, 1180−1182.
43. Lamzin, V. S., and Perrakis, A. (2000) Current state of automated crystallographic data analysis, *Nat. Struct. Biol. 7* (Suppl.), 978−981.
44. Lamzin, V. S., Perrakis, A., Bricogne, G., Jiang, J., Swaminathan, S., and Sussman, J. L. (2000) Apotheosis, not apocalypse: methods in protein crystallography, *Acta Crystallogr., Sect. D: Biol. Crystallogr. 56*, 1510−1511.
45. Jones, T. A., Zou, J. Y., Cowan, S. W., and Kjeldgaard. (1991) Improved methods for building protein models in electron density maps and the location of errors in these models, *Acta Crystallogr. A47*, 110−119.
46. Brunger, A. T., Kuriyan, J., and Karplus, M. (1987) Crystallographic *R* factor refinement by molecular dynamics, *Science 235*, 458−460.
47. Brunger, A. T., Adams, P. D., Clore, G. M., DeLano, W. L., Gros, P., Grosse-Kunstleve, R. W., Jiang, J. S., Kuszewski, J., Nilges, M., Pannu, N. S., Read, R. J., Rice, L. M., Simonson, T., and Warren, G. L. (1998) Crystallography & NMR system: A new software suite for macromolecular structure determination, *Acta Crystallogr., Sect. D: Biol. Crystallogr. 54*, 905−921.
48. Drozdzewski, P. M., and Johnson, M. K. (1988) A simple anaerobic cell for low temperature Raman spectroscopy, *Appl. Spectrosc. 42*, 1575−1577.
49. Hauptman, H. (1997) Phasing methods for protein crystallography, *Curr. Opin. Struct. Biol. 7*, 672−680.
50. Schlessman, J. L., Woo, D., Joshua-Tor, L., Howard, J. B., and Rees, D. C. (1998) Conformational variability in structures of the nitrogenase iron proteins from *Azotobacter vinelandii* and *Clostridium pasteurianum*, *J. Mol. Biol. 280*, 669−685.
51. Molloy, J. E., and Veigel, C. (2003) Biophysics. Myosin motors walk the walk, *Science 300*, 2045−2046.
52. Yildiz, A., Forkey, J. N., McKinney, S. A., Ha, T., Goldman, Y. E., and Selvin, P. R. (2003) Myosin V walks hand-over-hand: single fluorophore imaging with 1.5-nm localization, *Science 300*, 2061−2065.
53. Christiansen, J., Chan, J. M., Seefeldt, L. C., and Dean, D. R. (2000) The role of the MoFe protein α-125^{Phe} and β-125^{Phe} residues in *Azotobacter vinelandii* MoFe protein−Fe protein interaction, *J. Inorg. Biochem. 80*, 195−204.
54. Anderson, G. L., and Howard, J. B. (1984) Reactions with oxidized iron protein of *Azotobacter vinelandii* nitrogenase: formation of a 2Fe center, *Biochemistry 23*, 2118−2122.
55. Lindahl, P. A., Gorelick, N. J., Münck, E., and Orme-Johnson, W. H. (1987) EPR and Mössbauer studies of nucleotide-bound nitrogenase iron protein from *Azotobacter vinelandii*, *J. Biol. Chem. 262*, 14945−14953.
56. Fu, W., Morgan, T. V., Mortenson, L. E., and Johnson, M. K. (1991) Resonance Raman studies of the [4Fe-4S] to [2Fe-2S] cluster conversion in the iron protein of nitrogenase, *FEBS Lett. 284*, 165−168.
57. Spiro, T. G., Czernuszewicz, R. S., and Han, S. (1988) Iron−sulfur proteins and analogue complexes, in *Resonance Raman spectra of heme and metalloproteins* (Spiro, T. G., Ed.) pp 523−554, John Wiley & Sons, New York.
58. Fu, W., Drozdzewski, P. M., Adams, M. W. W., Morgan, T. V., Mortenson, L. E., LeGall, J., Peck, H. D., Jr., DerVartanian, D. V., and Johnson, M. K. (1993) Resonance Raman studies of iron-only hydrogenases, *Biochemistry 32*, 4813−4819.
59. Han, S., Czernuszewicz, R. S., Kimura, T., Adams, M. W. W., and Spiro, T. G. (1989) Fe_2S_2 protein resonance Raman spectra revisited: structural variations among adrenodoxin, ferredoxin, and red paramagnetic protein, *J. Am. Chem. Soc. 111*, 3505−3511.
60. Fu, W., Drozdzewski, P. M., Davies, M. D., Sligar, S. G., and Johnson, M. K. (1992) Resonance Raman and magnetic circular dichroism studies of reduced [2Fe-2S] proteins, *J. Biol. Chem. 267*, 15502−15510.
61. Johnson, M. K., Duin, E. C., Crouse, B. R., Golinelli, M.-P., and Meyer, J. (1998) Valence-delocalized $[Fe_2S_2]^+$ clusters in *Spectroscopic Methods in Bioinorganic Chemistry* (Solomon, E. I., and Hodgson, K. O., Eds.) pp 286−301, American Chemical Society, Washington, DC.
62. Broderick, J. B., Duderstadt, R. E., Fernandez, D. C., Wojtuszewski, K., Henshaw, T. F., and Johnson, M. K. (1997) Pyruvate formate-lyase activating enzyme is an iron−sulfur protein, *J. Am. Chem. Soc. 119*, 7396−7397.
63. Johnson, M. K., Staples, C. R., Duin, E. C., Lafferty, M. E., and Duderstadt, R. E. (1998) Novel roles for Fe-S clusters in stabilizing or generating radical intermediates, *Pure Appl. Chem. 70*, 939−946.
64. Pierrel, F., Hernandez, H., Johnson, M. K., Fontecave, M., and Atta, M. (2003) MiaB Protein from *Thermotoga maritima*: characterization of an extremely thermophilic tRNA-methylthiotransferase, *J. Biol. Chem. 278*, 29515−29524.
65. Agar, J. N., Krebs, B., Frazzon, J., Huynh, B. H., Dean, D. R., and Johnson, M. K. (2000) IscU as a scaffold for iron−sulfur cluster biosynthesis: sequential assembly of [2Fe-2S] and [4Fe-4S] clusters in IscU, *Biochemistry 39*, 7856−7862.
66. Krebs, C., Agar, J. N., Smith, A. D., Frazzon, J., Dean, D. R., Huynh, B. H., and Johnson, M. K. (2001) IscA, an alternate scaffold for Fe-S cluster biosynthesis, *Biochemistry 40*, 14069−14080.
67. Agar, J. N., Dean, D. R., and Johnson, M. K. (2003) Iron−sulfur cluster biosynthesis, in *Biochemistry and Physiology of Anaerobic Bacteria* (Ljungdahl, L. G., Adams, M. W. W., Barton, L. L., Ferry, J. G., and Johnson, M. K., Eds.) pp 46−66, Springer-Verlag, New York.

BI0358465